Wave Models

Gyroresonant wave particle interactions play a key role in radiation belt dynamics. Such interactions break the first and second adiabatic invariants leading to heating and acceleration by absorption of the waves and pitch angle scattering and loss to the atmosphere. Plasma waves that can lead to efficient gyroresonant wave particle interactions with energetic electrons include whistler mode chorus waves, plasmaspheric hiss, lightning-generated whistlers, magnetosonic waves and electromagnetic ion cyclotron waves.

Figure 1 shows an example of the rich variety of plasma waves typically observed in the inner magnetosphere in the frequency range from 100 Hz to 400 kHz. Here the wave electric field spectral intensity is plotted against UT for an entire orbit of the CRRES spacecraft. The solid white line shows the value of f_{ce} determined from the ambient magnetic field, and the dashed white lines below f_{ce} represent $0.5f_{ce}$, $0.1f_{ce}$, and the lower hybrid resonance frequency, f_{lhr}, respectively.

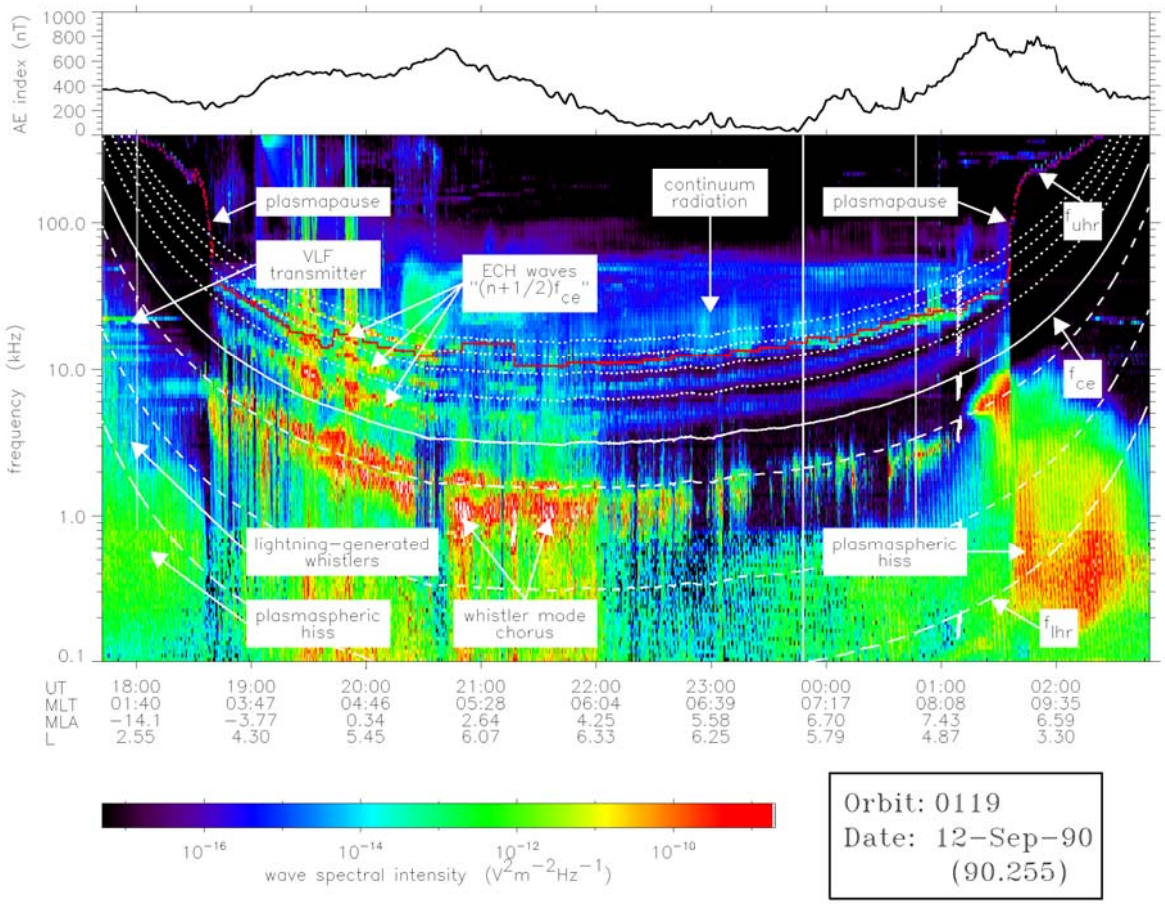

Figure 1 CRRES Wave Spectrogram for Orbit 119

Inside the plasmapause, on the outbound leg, weak nightside plasmaspheric hiss is observed below about 2 kHz while lightning generated whistlers contribute the weaker signal in the frequency range 2 kHz < f < 5 kHz. At higher frequencies, the horizontal lines between 10 and 25 kHz are from ground-based transmitters used for navigation and communication with submarines. Outside the plasmapause, which is crossed at 18:36 UT, the wave environment is very different. Strong upper and lower band whistler mode chorus emissions are observed below the electron gyrofrequency and weak electrostatic electron cyclotron harmonic (ECH) emissions are seen above the electron gyrofrequency. The chorus waves remain enhanced until about 2200 UT when the Auroral Electrojet (AE)index falls below 200 nT. Much weaker bursts of chorus are subsequently observed intermittently until the spacecraft reenters the plasmasphere on its inbound leg at 01:38 UT. In contrast, the ECH waves are observed to maximise near the magnetic equator and become much weaker as the spacecraft moves away from the equator and the magnetic activity drops. However, a combination of weaker ECH emissions and thermal noise are observed on the inbound pass right up until the spacecraft crosses the plasmapause at 01:38 UT. The chorus and ECH waves then abruptly cease and are replaced by strong dayside plasmaspheric hiss emissions below 2 kHz.

Dynamic global models of the radiation belts are diffusion models. They require diffusion rates that depend on wave properties. Since, as illustrated in Figure 1, wave properties can vary significantly with spatial location and geomagnetic activity the state of the art is to develop global models of the wave power for the various relevant wave modes using data from several satellites.

For SPACECAST we are combining plasma wave data from five different satellite missions (DE1, CRRES, Cluster 1, Double Star TC1 and THEMIS) and building new global models of the relevant plasma waves that both extend the coverage and improve the statistics of existing models. The new models will be used to compute new diffusion coefficients for use in the SPACECAST radiation belt models.

Figure 2 shows the distribution of (top) lightning generated whistlers and (bottom) plasmaspheric hiss inside the plasmasphere in the equatorial region ($-10^o < \lambda_m < 10^o$) as a function of L*, Magnetic Local Time (MLT) and geomagnetic activity. The geomagnetic activity is split into three activity levels using the AE index which is commonly used as a measure of substorm activity. We define the conditions as quiet when AE < 100 nT, moderate when 100 < AE < 300 nT and active when AE > 300 nT. The plots show the wave intensities as viewed from high above the Earth's north magnetic pole mapped to the magnetic equatorial plane with noon as at the top and dawn is to the right. The plots extend linearly out to L* = 10 with the strongest wave intensities coloured red and the weakest wave intensities coloured black.

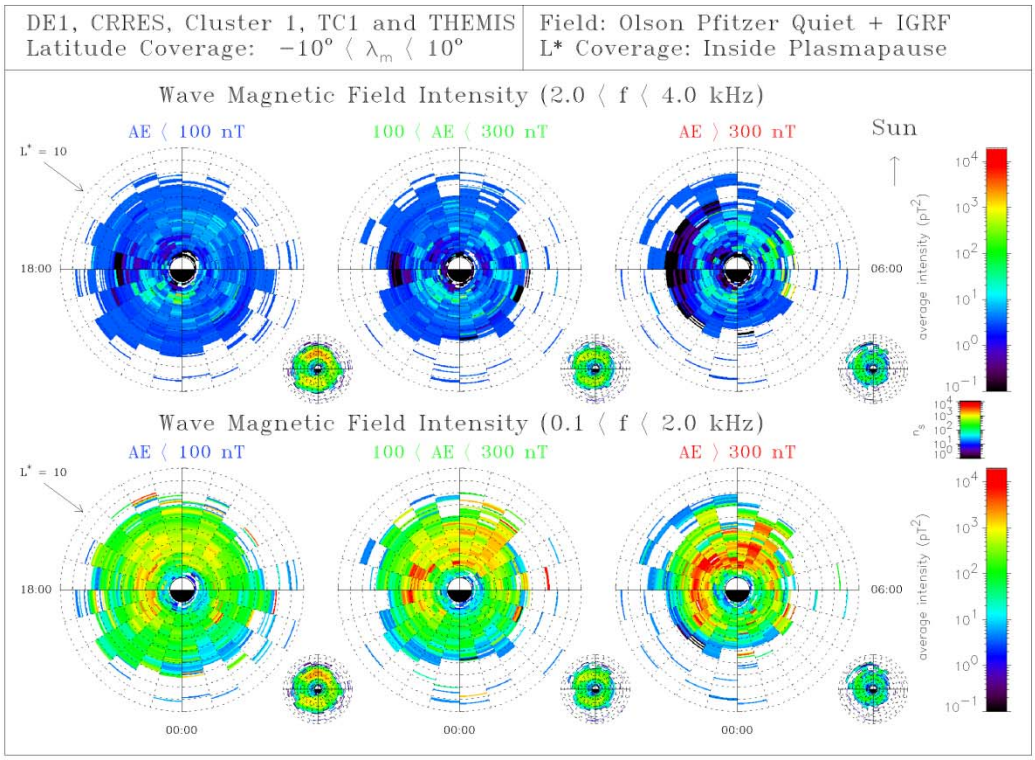

Figure 2 Combined satellite model of the equatorial wave intensity for (top) lightning generated whistlers and (bottom) plasmaspheric hiss as a function of L*, MLT and geomagnetic activity.

Plasmaspheric hiss is substorm dependent with the strongest emissions on the day-side, during active conditions. Here intensities can exceed 2000 pT^2 over a range of L*, typically in the region 2 < L* < 4. The emissions in the frequency band 2 < f < 4 kHz, attributed to lightning generated whistlers are much weaker and fall into two categories. The emissions on the nightside, between dusk and midnight show no substorm dependence and coincide with the region of strong lightning activity and weak D region absorption, confirming that these emissions are generated by lightning. In sharp contrast, on the dayside, the emissions are substorm dependent and have a similar distribution to plasmaspheric hiss, suggesting that these emissions may be weak, higher frequency hiss.

Figure 3 shows the distribution of (top) upper band chorus and (bottom) lower band chorus outside the plasmasphere in the equatorial region ($-10^o < \lambda_m < 10^o$) as a function of L*, MLT and geomagnetic activity. The chorus intensities are also substorm dependent with the largest intensities being seen in the lower-band with intensities of the order of 1000 pT^2 during active conditions in the region 4 < L* < 9 over a range of local times, primarily from 2300 MLT through dawn to 1200 MLT. Wave acceleraton is likely to be most effective in

this region. Equatorial upper-band chorus is both weaker and less extensive, with intensities of the order of a few hundred pT^2 during active conditions in the region $3 < L < 8$ over a similar range of local times.

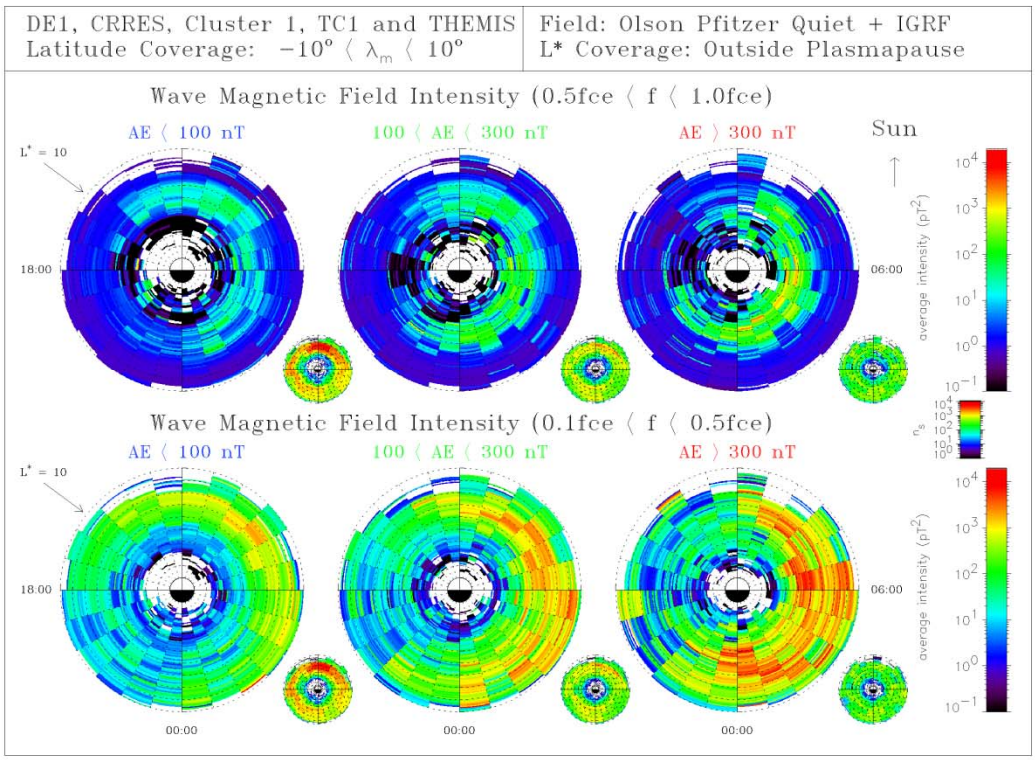

Figure 3 Combined satellite model of the equatorial wave intensity for (top) upper band chorus and (bottom) lower band chorus as a function of L*, MLT and geomagnetic activity.